Luminescence mechanisms of defective ZnO nanoparticles

Pietro Camarda,[ab] Fabrizio Messina,[a] Lavinia Vaccaro,[a] Simonpietro Agnello,[a] Gianpiero Buscarino,[a] Reinhard Schneider,[c] Radian Popescu,[c] Dagmar Gerthsen,[c] Roberto Lorenzi,[d] Franco Mario Gelardi,[a] and Marco Cannas*[a]

[a]*Dipartimento di Fisica e Chimica, Universita` di Palermo, Via Archirafi 36,*

I-90123 Palermo, Italia.

**E-mail: Marco.cannas@unipa.it*

[b]*Dipartimento di Fisica ed Astronomia, Universita` di Catania, Italia*

[c]*Laboratory for Electron Microscopy, Karlsruhe Institute of Technology,*

Engesserstrasse 7, 76131 Karlsruhe, Germany

[d]*Dipartimento di Scienza dei Materiali Universita` di Milano – Bicocca, Italia*

Abstract

ZnO nanoparticles (NPs) synthesized by pulsed laser ablation (PLAL) of a zinc plate in deionized water were investigated by time-resolved photoluminescence (PL) and complementary techniques (TEM, AFM, μRaman). HRTEM images show that PLAL produces crystalline ZnO NPs in wurtzite structure with a slightly distorted lattice parameter a. Consistently, optical spectra show the typical absorption edge of wurtzite ZnO (E_g = 3.38 eV) and the related excitonic PL peaked at 3.32 eV with a subnanosecond lifetime. ZnO NPs display a further PL peaking at 2.2 eV related to defects, which shows a power law decay kinetics. Thermal annealing in O_2 and in a He atmosphere produces a reduction of the A_1(LO) Raman mode at 565 cm^{-1} associated with oxygen vacancies, accompanied by a decrease of defect-related emission at 2.2 eV. Based on our experimental results the emission at 2.2 eV is proposed to originate from a photo-generated hole in the valence band recombining with an electron deeply trapped in a singly ionized oxygen vacancy. This investigation clarifies important aspects of the photophysics of ZnO NPs and indicates that ZnO emission can be controlled by thermal annealing, which is important in view of optoelectronic applications.

Introduction

Zinc oxide is a wide band gap semiconductor with great potential for a variety of practical applications, such as piezoelectric transducers, photovoltaics, transparent electrodes, gas sensors, bioimaging probes, drug delivery, light emitters and photocatalysis.[1–7] In fact, its direct band-gap (3.37 eV in bulk form) and large exciton-binding energy (60 meV)[1] make ZnO especially promising for photonic applications in the UV or blue spectral range even at room temperature. A great variety of chemical and physical methods have been used to produce ZnO NPs (chemical reduction of metal ions, sputtering, molecular beam epitaxy and electron beam deposition).[8–10] Among them, pulsed laser ablation in liquids (PLAL) offers a simple and versatile route to synthesize NPs of extremely high purity.[11–18] In this technique, NPs form by interaction between a bulk target immersed in liquid medium and a pulsed laser beam; in particular, ZnO NPs can be produced by ablating a zinc metal plate in water.[2,19,20] Hence, the ablation conditions play the most significant role in controlling the morphology and properties of the nanoparticles. By changing laser photon energy, fluence, pulse duration, solvent and solute, different morphologies and structures can be obtained.[16,21–23]

In addition to the near-UV excitonic emission peak (3.3 eV), ZnO exhibits visible luminescence in the yellow-orange region which has been assigned to interstitial oxygen and dislocation, as well as Li dopants[1] and another emission in the green region, the origin of which is not conclusively settled.[24–26] It should be noted that the reported peak position of the green emission differs from one study to another (2.2–2.4 eV)[26] and different positions, in some cases, are assigned to different defects.[24] Proposed hypotheses on the origin of this green emission include zinc vacancies, oxygen antisites, oxygen vacancies and surface defects.[3,26–33] For example, zinc vacancies were related to green PL at 2.3 eV in bulk ZnO comparing the PL spectra for the samples with different Zn and O implantations,[31] instead, oxygen antisites were assumed to explain PL at 2.4 eV in ZnO films based on the increase of green PL caused by annealing in O_2.[32] Anyway, the most common attribution remains the singly ionized oxygen vacancy based on the correlation between structural properties and green PL intensity.[27–29,34,35] In particular, two likely mechanisms for the ZnO visible emission have been suggested: one is the recombination of a shallowly trapped electron with a hole in a deep trap,[34,36] and the other is the recombination of an electron in singly occupied oxygen vacancies with a photo-generated hole in the valence band.[35,37]

All experiments reported so far to study the optical properties of ZnO NPs lack a complete characterization with time-resolved PL measurements, which is mandatory to obtain a comprehensive view of the photophysics of luminescence defects or excitons and, in particular, of the emission mechanism responsible for the green PL. A thorough understanding of the origin

of the PL signals is needed to control the emission capabilities of ZnO NPs produced by PLAL, which is important for optoelectronic applications. To this aim, one needs to obtain a thorough picture of the structural, morphological and optical properties of the produced ZnO NPs, a task which can only be achieved combining several experimental techniques. Moreover, thermal treatments in a controlled atmosphere can be used as an additional method to give more information. In this work we investigate ZnO NPs produced by PLAL of a zinc plate in water by an experimental approach based on the use of time-resolved luminescence and complementary techniques, such as transmission electron microscopy (TEM), atomic force microscopy (AFM), μRaman, thermal treatments in controlled atmospheres, used to probe the morphological and structural properties, thus providing a solid support to discuss the origin of the observed PL bands.

Experimental methods

The synthesis of ZnO NPs was carried out by ns PLAL. A zinc plate with a thickness of 0.5 mm, used as a target, was placed at the bottom of a vessel containing deionized water (10 ml). The first harmonic (λ = 1064 nm) of a pulsed Nd:YAG laser (Quanta System SYL 201) operating at a repetition rate of 10 Hz, with a pulse width of 5 ns and 90 mJ per pulse energy, was weakly focused by a lens (focal length = 10 cm) on the Zn target (spot size ≈2 mm), which was continuously moved via a rotator plate to avoid the laser beam from always hitting the same area and forming craters. The irradiation time was 15 minutes corresponding to a total fluence of 25.8 kJ cm^{-2}. Atomic force microscopy (AFM) measurements in air were done by two different instruments: a Bruker FAST-SCAN microscope working in the soft tapping mode and using a FAST-SCAN-A probe with an apical radius of about 5 nm, and a multimode V (Veeco Metrology) scanning microscope working in the tapping mode and using a commercial silicon probe having a tip radius <10 nm. All images were acquired on a dried droplet deposited onto a mica substrate. The structure of the produced nano particles was characterized by both high resolution TEM (HR-TEM), selected-area electron diffraction (SAED) and μRaman spectroscopy. HRTEM images were obtained using an aberration-corrected FEI Titan 380–300 microscope at 300 kV acceleration tension. The specimens were prepared by dropping the ablated solution over a holey carbon-film copper-grid at room temperature in air. Confocal microscopy and Raman spectroscopy were performed using a Bruker SENTERRA spectrometer (λ = 532 nm, power 20 mW), supplied with a CCD camera and a microtranslation stage, with the maximum spectral resolution being 3 cm^{-1}. The UV-Vis optical absorption (OA) spectra were recorded using a double beam spectrometer (JASCO V-560) in a 0.5 cm optical path quartz cell (spectral resolution 2 nm). Time resolved PL spectra of the colloidal solution in a quartz cell (1 cm optical path) were excited using a tunable laser consisting of an optical parametric oscillator pumped by the third harmonic of a Nd:YAG laser. The emitted light was analyzed using a monochromator (with two

gratings of 150 or 300 lines per mm and a blaze wavelength of 300 or 500 nm) and acquired by an intensified CCD camera driven by a delay generator (PI MAX Princeton Instruments) setting the acquisition time window, T_W, and the delay, T_D, with respect to the arrival of laser pulses. Time-correlated single photon counting measurements were carried out using a FLS 980 spectrofluorometer equipped with a pulsed diode light source (EPLED by Edinburgh Photonics, pulse duration 900 ps, excitation wavelength 250 nm) and collecting the signal at 373 nm with a bandpass of 20 nm. The photo luminescence excitation (PLE) spectra were measured using a spectrofluorometer (JASCO FP-6500) and corrected for the intensity distribution of the excitation xenon lamp.

Results and discussion

During the PLAL experiments it is observed that the colorless liquid changed to a coloured suspension, indicating the production of NPs. At the end of 15 min PLAL, we obtained a brownish colloidal solution, which gradually changes to pale yellow in tens of minutes. The results here reported have been obtained on the stable colloidal solution. The AFM image and particle size distribution of NPs are shown in Fig. 1(a) and (b).

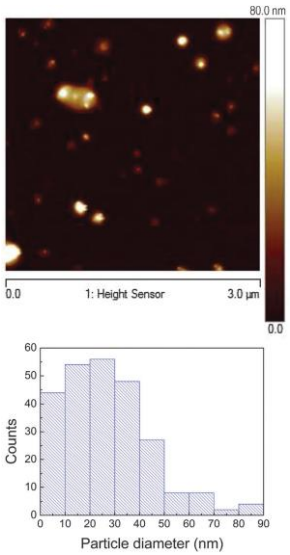

Fig. 1 (a) AFM image 3 x 3 µm^2 of the dried colloidal solution of ZnO NPs produced by PLAL; (b) size distribution calculated from the AFM image.

They reveal that the ablation product consists of a broad distribution of spherical-like nanoparticles with sizes ranging from about 5 nm to 90 nm and with an average size of about 30 nm. Fig. 2(a) displays the typical HRTEM images of two nanoparticles with d = 30 nm and d = 50 nm respectively, which highlight the formation of crystalline NPs.

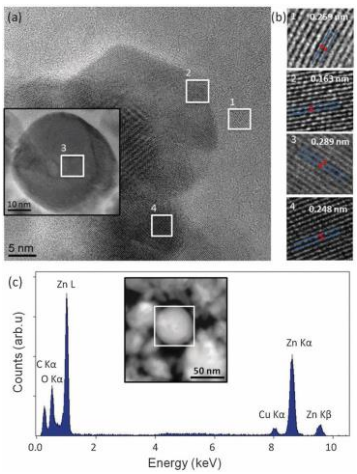

Fig. 2 (a) HRTEM images of two typical ZnO NPs with d = 30 nm (main panel) and 50 nm (inset); (b) magnified images of selected regions in (a) which show the crystalline planes of the nanoparticle; (c) HAADF image of the NPs highlighting the area used for the EDXS analysis (square region) and the corresponding area-EDX spectrum.

The magnified square regions of the nanoparticles (Fig. 2(b)) evidence that the distances between adjacent lattice planes are 0.259 ± 0.001 nm, 0.1630 ± 0.0006 nm, 0.289 ± 0.001 nm and 0.248 ± 0.002 nm, which are consistent with the (002), (110), (100) and (101) crystalline plane distances of ZnO in the wurtzite structure, respectively. It is worth noting that the (100) distance, 0.289 nm in our case, is slightly larger than the measured value for bulk ZnO (0.281 nm).[38] This finding can be attributed to a larger lattice parameter *a* = 0.334 ± 0.001 nm as compared to the expected value of 0.325 nm. It is known that in highly defective nano materials the lattice constants can be slightly different with respect to the bulk material;39 for example, Zeng and co-workers showed a deviation in the ZnO(100) lattice distance from the normal value in highly defective ZnO NPs produced by PLAL.28 Further information on NPs can be derived by using high-angle annular dark-field imaging (HAADF) TEM combined with Energy-dispersive X-ray spectroscopy (EDXS). The Zn and O content within a single large nanoparticle are determined from EDXS line analysis, by scanning a square region within single NPs. Fig. 2(c) shows the HAADF image of a nanoparticle with *d* = 50 nm within the same square region. The EDX spectrum reported in Fig. 2(c) reveals the characteristic X-ray lines of Zn-K, Zn-L and O-K series, besides the lines of Cu-K series from the grid and C-K from the amorphous substrate.

The quantification of Zn and O content results in an average chemical composition of $Zn_{0.47–0.43}O_{0.53–0.57}$ for the NPs, which is consistent with the chemical composition of ZnO.[40] The small increase of the O content within the nanoparticle as compared to that of ZnO, could be attributed to H_2O and O_2 molecules trapped inside the ZnO NPs during the formation processes involved in PLAL. However, a minor contribution due to the presence of oxygen on the amorphous substrate cannot be excluded. The OA and PL spectra of ZnO NPs dispersed in water are shown in Fig. 3(a) and (b).

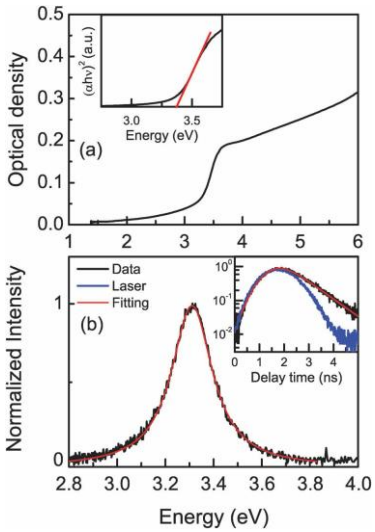

Fig. 3 (a) UV-Vis optical absorption of the colloidal solution; (b) ZnO exciton PL excited at 4.66 eV, fitted by a Lorentzian curve (red solid line); the inset in (a) shows the Tauc plot of the absorption spectrum in the hypothesis of the direct band-gap; the inset in (b) shows the time decay curve of the exciton PL. The smooth solid line represents the best fit to the PL decay using a convolution function between a single exponential and the instrument response function (blue line).

The absorption spectrum shows the typical edge of ZnO, from which we estimate the optical band-gap of 3.38 ± 0.01 eV by extrapolating the linear region observed in a Tauc plot (reported in the inset of Fig. 3(a)), as expected for direct allowed transitions.[41] Such a value is consistent with that of a bulk ZnO crystal in the wurtzite structure.[42] The UV emission reported in Fig. 3(b), excited at 4.66 eV and detected with a time window T_W = 10 ns and a time delay T_D = 0 ns with respect to the arrival of laser pulses, has a Lorentzian shape with a FWHM of 0.20 eV and peaked at 3.32 ± 0.01 eV; we note that this value is 60 meV below the optical band-gap obtained from the OA spectrum, matching the value of the exciton binding energy E_b in wurtzite ZnO. We observe that, despite the fact that nanoparticle size distribution is quite wide, there is no effect on the luminescence spectrum since almost all NPs are larger than the excitonic Bohr radius (2.34 nm).[1] This PL band is characterized by a sub

nanosecond lifetime, hence, in order to estimate the exciton lifetime it is mandatory to take into account the instrument response using a fitting function which consists of the convolution between a single exponential decay function, exp(-t/τ), and a Gaussian curve taking into account the laser profile. Based on this procedure, the inset in panel (b) shows the time decay curve of the PL band and the best fit function to the PL decay from which we obtain the life time of the exciton PL, τ = 800 ± 100 ps. This value is much smaller than the reported value in high quality bulk ZnO materials, which reaches several nanoseconds;[43,44] it substantially agrees with the lifetime in the range of hundreds of picoseconds found in ZnO nanostructures.[45–48] In these studies, authors suggested that the exciton lifetime is largely determined by non-radiative recombination due to a high defect density, although no obvious correlation was found between the excitonic PL decay times and the defect emission intensities.[45] Time resolved PL allows distinguishing between two different contributions (excitons and defects) of the spectrum, under the same excitation energies. The PL spectrum of Fig. 4, excited at 4.66 eV and detected with T_W = 10 ms and T_D = 20 ns, shows a broad green emission centered at 2.2 eV.

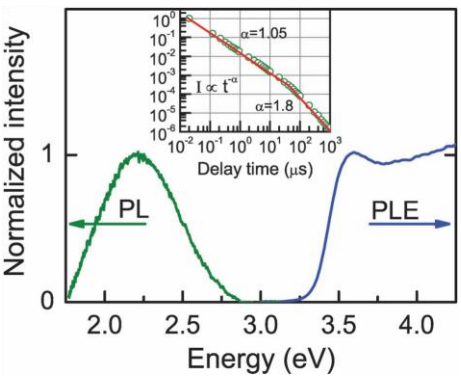

Fig. 4 Defect related PL of ZnO excited at 4.66 eV and a normalized excitation spectrum (PLE) monitored at 2.15 eV; the inset shows the time decay curve of the defect related PL; the smooth solid line represents the best fit linear curve.

The PLE spectrum exhibits a sharp threshold at ≈3.5 eV and appears almost flat at higher energies. This shape indicates that the green band is excited only by photon energies larger than the band-gap, thus suggesting that the excitation initially involves a band-to-band transition producing a free electron–hole pair. The inset of Fig. 4 reports the time decay curve of the PL band in a log/log scale. Data follow two different linear trends consistent with power law time dependence $I \propto t^{-\alpha}$ across 5 decades of time; the first one in the region from 20 ns to 40 μs and the second one from 40 μs up to 1 ms. By a fitting procedure we get α = 1.05 ± 0.05 and α = 1.8 ± 0.1 for the two ranges of time, therefore the decay kinetics of the green band follow a power law with $I \propto t^{-1.05}$ from 20 ns to 40 μs and a different power law with $I \propto t^{-1.8}$ from 40 μs to 1 ms. We observe that, in contrast with

previous studies,[49,50] the decay kinetic does not change varying the excitation energy in the whole range of the excitation spectrum (from 3.3 to 5 eV). A power law decay kinetics of the PL intensity with $\alpha \approx 1$ has been observed in self-trapped excitons in irradiated single crystals of anatase TiO_2 and attributed to tunneling recombination of trapped electrons and holes.[51] In a recent work Huntley[52] has shown that a power law of the PL decay with $\alpha = 1–1.5$ can result from the tunnelling of trapped electrons to recombination centres which are randomly distributed in space. Instead, the power law decay for $t > 40$ μs nearly matches the hyperbolic t^{-2} time dependence typical of bimolecular recombination for a balanced donor–acceptor system.[53,54] Such behavior suggests that the defect PL decay in the first three decades of time is driven by tunneling of trapped carriers to recombination centres ($\alpha = 1.05$); however, for a sufficiently larger time ($t > 40$ μs) most of the electrons or holes come out from their trap, thus the main mechanism becomes a bimolecular recombination ($\alpha = 1.8$).

Up to now, many point defects have been suggested for the green emission, including oxygen vacancies, antisite oxygen, zinc vacancies, zinc interstitials, and surface states.[3,26,33] The most popular attribution of this visible PL is to oxygen vacancies.[27–29] Since ZnO NPs were synthesized by PLAL in water of a Zn plate, they are formed under Zn-rich conditions; thus the most likely defect types are oxygen vacancies and zinc interstitials, having the lowest formation energy.[1,5] However, PL and PLE in contrast with the expected results correspond to zinc interstitials in ZnO NPs. In fact, Zeng and co-workers reported a PL band, attributed to zinc interstitial, peaked at 2.8 eV in ZnO NPs produced by PLAL in water of a Zn plate,[28,55] which is at larger energy compared to the 2.2 eV PL band showed in this work. Besides, the PLE spectrum of this blue PL reveals a peak at energy close to the band-gap (3.2 eV) and also a slowly dropping tail, which continues into the violet region, very different with respect to the sharp-edged green PLE in the UV region described above.[28] Recently, we have provided evidence about the attribution of the green PL to oxygen vacancies.[30] In that work, we acquired online optical measurements (OA and PL) during nanosecond PLAL of a Zn plate in water. We proposed that the growth of defective ZnO NPs is the result of aqueous oxidation of Zn NPs, out of the plume region, slowed down and hindered by water diffusion through the ZnO shell. This causes an incomplete oxidation of zinc leading to slightly substoichiometric ZnO NPs rich in oxygen vacancies. Here, in order to further verify this assignment we performed thermal treatment on the dried colloidal solution of ZnO NPs at 300 °C at 100 bar of oxygen or in an inert helium atmosphere. The morphological and structural properties of the treated ZnO NP powder in an O_2 atmosphere are reported in Fig. 5(a) and (b), respectively.

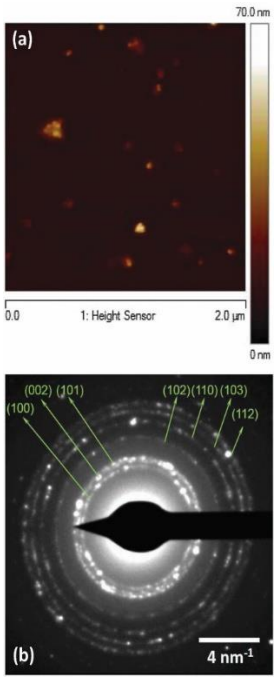

Fig. 5 (a) AFM image 2x2 µm^2 of ZnO NPs taken after thermal treatments at 300 °C at 100 bar of oxygen. (b) SAED pattern obtained from a selected area of a HRTEM image containing several ZnO NPs, arrows indicate the lattice planes of ZnO in the wurtzite structure.

The AFM image shows that NPs maintain the size of tens of nanometers as for the untreated sample. Moreover, the SAED pattern demonstrates that ZnO NPs are crystalline and all observed Debye–Scherrer rings can be attributed to the hexagonal ZnO with lattice parameters a = 0.325 nm and c = 0.521 nm. Thus, NPs after thermal treatments preserve their crystalline structure and in addition the lattice parameter a tends to the reported value for defect free ZnO. These results demonstrate that treatment does not produce a significant variation in the structure and particle sizes. The same results have been obtained for ZnO NPs treated in a He atmosphere. Fig. 6 reports the green PL band of the ZnO powder acquired before and after thermal treatment in oxygen and in a helium atmosphere.

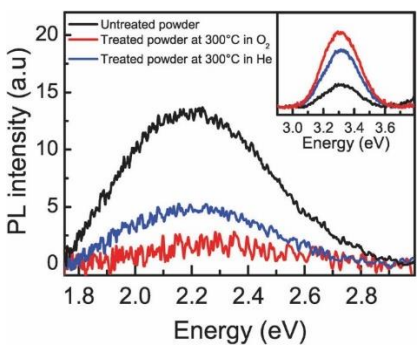

Fig. 6 Defect PL, excited at 4.66 eV, of the ZnO NPs powder produced by PLAL acquired before and after thermal treatment at 300 °C at 100 bar of oxygen (red line) and in a helium (blue line) atmosphere; the inset shows an excitonic band of the ZnO NPs dissolved in water, acquired before and after thermal treatments.

We note that the excitonic PL is not detected in the powder form of the sample: we suggest that it is quenched by aggregation of NPs. Thus, to acquire the excitonic PL we dissolved the powder of ZnO NPs (treated and untreated) in deionized water. The inset shows excitonic PL, normalized for the optical density at the excitation energy (4.66 eV), acquired before and after the thermal treatments of the powder dissolved in water. The PL measurements of the two signals were performed using the same time parameters as provided in Fig. 3 and 4. It is evident that the intensity of the green band after thermal annealing in oxygen decreases by about seven times compared to the as grown powder. In addition, we observe a concurrent increase of a factor of three of the excitonic luminescence. In general, competition of the green- and the excitonic-PL emissions is found in ZnO. When the green band is strong, the excitonic band tends to be small or absent and conversely.[27,47,56,57]

The μRaman spectra of the ZnO NPs acquired before and after thermal treatments are reported in Fig. 7. Raman peaks at 334 cm^{-1}, 438 cm^{-1}, and 565 cm^{-1} correspond to $E^{(2)}{}_2$, $E^{(2)}{}_2$-$E^{(1)}{}_2$ and A_1(LO) modes of ZnO in the wurtzite structure.[58]

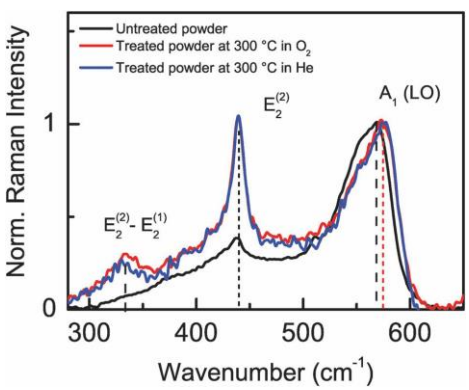

Fig. 7 mRaman spectrum of the ZnO NPs produced by PLAL acquired before and after thermal treatment at 300 °C at 100 bar of oxygen (red line) and in a helium (blue line) atmosphere. Raman intensity are normalized to the difference between the intensities of the A_1(LO) Raman peak and background.

The most evident change in the Raman spectra induced by thermal annealing involves the intensity of the peak at 565 cm^{-1} accompanied by a blue shift up to 573 cm^{-1} which is the expected value for ZnO Bulk. This peak, which dominates the spectrum of untreated ZnO NPs, reduces by a factor of six after thermal treatment. It is worth noting that this mode is almost negligible in bulk ZnO, which is due to the cancelation between the deformation and Fröhlich contributions to the LO phonon scattering cross section.[59] However, oxygen vacancies or zinc interstitials or their complexes are assumed to enhance the A_1(LO)

mode.[57,60–63] Indeed, since our ZnO NPs are rich in defects, as usual in most ZnO nanostructured materials, this peak is prominent compared to the $E^{(2)}_2$ mode.[58] In ZnO films fabricated under different O_2 pressures, the Raman peak at 579 cm^{-1} is reported to decrease with the increase of O_2 pressure.[61] This is ascribed to the reduction of defect states. For ZnO single crystals, implantation of P ions is reported to increase oxygen vacancies and to enhance the Raman peak at 575 cm^{-1}.[60] Overall, the decrease of the A_1(LO) peak (Fig. 7), the reduction of defect PL (Fig. 6) and the increase of the excitonic PL (inset of Fig. 6), observed here upon treatment in O_2, can be explained as an effect of the reduction of oxygen vacancies. Rather unexpectedly, we found that thermal treatments in a He atmosphere also cause the same reduction of the A_1(LO) peak (see Fig. 7), but they produce a different quantitative effect on the optical properties of the ZnO NPs. In particular, we obtained an intermediate reduction of the green PL (a factor of three) with respect to the oxygen atmosphere (a factor of seven) and a weaker increase of the excitonic PL (as from Fig. 6). This annealing effect in a He atmosphere can be explained considering that H_2O or O_2 could already be present and trapped inside the ZnO NPs left by their formation processes involved during and after PLAL. Consistently, the EDX spectrum shown in Fig. 2c reveals an excess of oxygen for the ZnO NPs. During thermal treatments, these molecules can diffuse through the NPs completing the oxidation process and hence reducing the concentration of oxygen vacancies in ZnO NPs; this leads to the decrease of both green PL and the A_1(LO) mode and the increase of the exciton PL. In the case of thermal annealing in an oxygen atmosphere we add oxygen molecules which enter the NPs; this process induces a further oxidation and consequently a further reduction of the oxygen vacancies. Consistently we observe a further decrease of the green PL and a concurrent further increase of the excitonic PL.

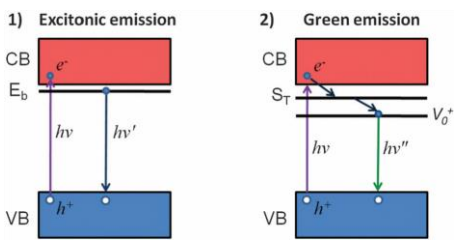

Fig. 8 Photoluminescence processes suggested for ZnO NPs: (1) typical exciton emission; (2) recombination of a shallowly trapped hole with a deeply trapped electron into singly ionized oxygen vacancies.

On the basis of our experimental results we propose two mechanisms leading to PL emissions (illustrated in Fig. 8): one is the typical exciton emission or near-band-edge emission, i.e., photo-generated electrons recombine with holes in the valence band or in traps near the VB, producing the PL band peaked at 3.32 eV with a lifetime of about 800 ps. As for the visible emission

at 2.2 eV related to the oxygen vacancies, the recombination occurs between a hole in the VB and an electron deeply trapped in a singly ionized oxygen vacancy. The energy level of this oxidation state of the oxygen vacancies has been calculated by Janotti and co-workers by density-functional calculations to be about 1 eV below the CB,[5] which is consistent with the peak position of the green PL. We observe that this emission mechanism for the green PL is different from previously proposed models consisting of a recombination involving free electrons in the CB with double-defect centers (oxygen vacancy + zinc vacancy) above the VB,[36] or oxygen vacancies indirectly assisted by zinc interstitials.[37] Finally, in order to take into account the power law decay discussed above, we propose the electron to be temporarily trapped in an unknown trap state (S_T in Fig. 8). From this state, the electron tunnels into a double ionized oxygen vacancy which becomes a singly ionized oxygen vacancy defect.

Conclusions

ZnO NPs with an average size of 30 nm were synthesized by PLAL of a zinc plate in deionized water and characterized by time-resolved luminescence and complementary techniques (TEM, AFM, μRaman). HRTEM images show crystalline ZnO NPs in the wurtzite structure with a change in the nanocrystal lattice parameter a as indicated by a larger distance between (100) lattice planes. Consistently, optical absorption and time resolved PL spectra show the typical absorption edge of the wurtzite ZnO (E_g = 3.38 eV) and the relative excitonic fast PL peaked at 3.32 eV with a single exponential lifetime of about 800 ps. In addition, we observed a visible PL at 2.2 eV due to the presence of defects in ZnO NPs with a sharp edged excitation spectrum and a power law decay time, which indicates that the recombination is driven by tunnelling of trapped electrons to recombination centres randomly distributed in space. Thermal annealing at 300 °C in an O_2 atmosphere, and to a smaller extent, even in a He atmosphere, produces a reduction of the A_1(LO) mode at 565 cm^{-1}, which is related to oxygen vacancies.

Moreover, thermal treatments lead to a decrease of the green PL demonstrating the relation between oxygen vacancies and the green PL in ZnO NPs, while the excitonic luminescence at 3.32 eV is enhanced. Based on our experimental results we propose a recombination mechanism responsible for the green PL involving a hole in the VB recombining with a deeply trapped electron in singly ionized oxygen vacancies. Besides providing additional information on the origin and mechanism of the green PL, these results underscore the possibility of controlling the intensity of the PL bands of ZnO NPs by thermal annealing procedures.

Acknowledgements

This work was partially supported by FAE project, PO FESR Sicilia 2007/2013 4.1.1.1 and FFR 2012/2013 of University of Palermo. We express our gratitude to the group of the Laboratory of Advanced Materials Physics (Palermo University) (http://www. unipa.it/lamp/) for the valuable and stimulating discussions. G. Napoli and G. Tricomi are acknowledged for their technical assistance. Roberto Lorenzi acknowledges the financial support of CARIPLO Foundation under project 2012-0920. The CHAB laboratories are acknowledged for the AFM equipment use (http://www.chab.center/home, Microscopy and Bioimaging Lab, PONa3 00273, University of Palermo). This research received support from the QualityNano Project http://www.qualitynano.eu/financed by European Community Research Infrastructure Action under the FP7 ‘‘Capacities’’ Program.

References

1 U. Ozgur, I. Alivov, C. Liu, A. Teke, M. A. Reshchikov, S. Dogan, V. Avrutin, S. J. Cho and H. Morkoc, J. Appl. Phys., 2005, 98, 041301.

2 J. M. Cho, J. K. Song and S. Park, Bull. Korean Chem. Soc., 2009, 30, 1616–1618.

3 Z. Zhang and H. Xiong, Materials, 2015, 8, 3101–3127.

4 J. Song, S. A. Kulinich, J. Li, Y. Liu and H. Zeng, Angew. Chem., Int. Ed., 2015, 54, 462–466.

5 A. Janotti and C. G. V. de Walle, Rep. Prog. Phys., 2009, 72, 126501.

6 X. Gao, Y. Cui, R. M. Levenson, L. W. K. Chung and S. Nie, Nat. Biotechnol., 2004, 22, 969–976.

7 Y. Kozuka, A. Tsukazaki and M. Kawasaki, Appl. Phys. Rev., 2014, 1, 011303.

8 L. Schmidt-Mende and J. L. MacManus-Driscoll, Mater. Today, 2007, 10, 40–48.

9 B. B. Straumal, S. G. Protasova, A. A. Mazilkin, B. Baretzky, A. A. Myatiev, P. B. Straumal, T. Tietze, G. Schutz and E. Goering, Mater. Lett., 2012, 71, 21–24.

10 S. C. Singh and R. Gopal, Physica E, 2010, 40, 724–730.

11 F. Mafune´, J. Y. Kohno, Y. Takeda and T. Kondow, J. Phys. Chem. B, 2000, 104, 8333–8337.

12 F. Mafune´, J. Y. Kohno, Y. Takeda and T. Kondow, J. Phys. Chem. B, 2003, 107, 4218–4223.

13 C. Liang, Y. Shimizu, T. Sasaki and N. Koshizaki, J. Phys. Chem. B, 2003, 107, 9220–9225.

14 Z. Yan and B. Chrisey, J. Photochem. Photobiol., C, 2012, 13, 204–223.

15 H. Zeng, X. W. Du, S. C. Singh, S. A. Kulinich, S. Yang, J. He and W. Cai, Adv. Funct. Mater., 2012, 22, 1333–1353.

16 R. Intartaglia, K. Bagga, M. Scotto, A. Diaspro and F. Brandi, Opt. Mater. Express, 2012, 2, 510–518.

17 L. Vaccaro, L. Sciortino, F. Messina, G. Buscarino, S. Agnello and M. Cannas, Appl. Surf. Sci., 2014, 302, 62.

18 T. Sasaki, Y. Shimizu and N. Koshizaki, J. Photochem. Photobiol., A, 2006, 182, 335–341.

19 R. I. Ismail, A. K. Ali, M. M. Ismail and K. I. Hassoon, Appl. Nanosci., 2011, 1, 45–49.

20 R. K. Thareja and S. Shukla, Appl. Surf. Sci., 2007, 253, 8889–8895.

21 E. Fazio, A. Mezzasalma, G. Mondio, F. Neri and R. Saija, Appl. Surf. Sci., 2013, 272, 30–35.

22 E. Solati, Opt. Laser Technol., 2014, 58, 26–32.

23 K. K. Kim, D. Kim, S. K. Kim, S. M. Park and J. K. Song, Chem. Phys. Lett., 2011, 511, 116–120.

24 M. M. Cluskey and S. Jokela, J. Appl. Phys., 2009, 106, 071101.

25 A. Djuris˘ic´, X. Chen, Y. Leung and A. Ng, J. Mater. Chem., 2012, 22, 6526–6535.

26 A. Djuris˘ic´, A. Ng and X. Chen, Prog. Quantum Electron., 2010, 34, 191–259.

27 K. Kawabata, Y. Nanai, S. Kimura and T. Okuno, Appl. Phys. A: Mater. Sci. Process., 2012, 107, 213–220.

28 H. Zeng, G. Duan, Y. Li, S. Yang, X. Xu and W. Cai, Adv. Funct. Mater., 2010, 20, 561–572.

29 R. S. Ajimsha, G. Anoop, A. Aravind and M. K. Jayarajz,

Electrochem. Solid-State Lett., 2008, 11, k14–k17.

30 P. Camarda, L. Vaccaro, F. Messina and M. Cannas, Appl. Phys. Lett., 2015, 107, 013103.

31 Q. X. Zhao, P. Klason, M. Willander, H. M. Zhong, W. Lu and J. H. Yang, Appl. Phys. Lett., 2005, 87, 211912.

32 B. Lin, Z. Fu and Y. Jia, Appl. Phys. Lett., 2001, 79, 943.

33 F. Fabbri, M. Villani, A. Catellani, A. Calzolari, G. Cicero,

D. Calestani, G. Calestani, A. Zappettini, B. Dierre,

T. Sekiguchi and G. Salviati, Sci. Rep., 2014, 4, 5158. 34 A. V. Dijken, E. A. Meulenkamp, D. Vanmaekelbergh and A. Meijerink,

J. Lumin., 2000, 87, 454–456.

35 L. Zhang, L. Yin, C. Wang, N. lun, Y. Qi and D. Xiang, J. Phys. Chem. C, 2010, 114, 9651–9658.

36 M. Li, G. Xing, G. Xing, B. Wu, T. Wu, X. Zhang and T. C. Sum, Phys. Rev. B: Condens. Matter Mater. Phys., 2013, 87, 115309.

37 K. Kodama and T. Uchino, J. Appl. Phys., 2012, 111, 093525. 38 K. Kihara and G. Donnay, Can. Mineral., 1985, 23, 647–654.

39 A. F. Kohan, G. Ceder, D. Morgan and C. G. V. de Walle, Phys. Rev. B: Condens. Matter Mater. Phys., 2000, 61, 15019–15027.

40 B. C. Lin, P. Shen and S. Y. Chen, J. Phys. Chem. C, 2011, 115, 5003–5010.

41 J. Tauc, R. Grigorovici and A. Vancu, Phys. Status Solidi, 1966, 15, 627.

42 C. Klingshirn, ChemPhysChem, 2007, 8, 782–803.

43 T. Koida, A. Uedono, A. Tsukazaki, T. Sota, M. Kawasaki and S. F. Chichibu, Phys. Status Solidi A, 2004, 201, 2841–2845.

44 S. F. Chichibu, T. Onuma, M. Kubota, A. Uedon and T. Sota, J. Appl. Phys., 2006, 99, 093505.

45 W. M. Kwok, A. B. Djurisica, Y. H. Leung, W. K. Chan and D. L. Phillips, Appl. Phys. Lett., 2005, 87, 223111.

46 S. K. Mohanta, D. C. Kim, X. H. Zhang, C. B. Soh, A. M. Yong, H. K. Cho and S. Tripathy, J. Cryst. Growth, 2008, 310, 5312.

47 H. C. Hsu, H. Y. Huang, M. O. Eriksson, T. F. Dai and
P. Holtz, Appl. Phys. Lett., 2013, 102, 013109.

48 F. Jen, Y. Lu, C. Chen, H. Wang and C. C. Yang, Appl. Phys. Lett., 2005, 87, 252117.

49 K. Kodama and T. Uchino, J. Phys. Chem. C, 2014, 118, 23977.

50 A. van Dijken, E. A. Meulenkamp, D. Vanmaekelbergh and A. Meijerink, J. Phys. Chem. B, 2000, 104, 1715. 51 M. Watanabe, S. Sasaki and T. Hayashi, J. Lumin., 2000, 87, 1234–1236.

52 D. J. Huntley, J. Phys.: Condens. Matter, 2006, 18, 1359–1365.

53 D. G. Thomas, J. J. Hopfield and W. M. Augustyniak, Phys. Rev., 1965, 140, A202.

54 V. N. Sigaev, N. V. Golubev, E. S. Ignat'eva, A. Paleari and R. Lorenzi, Nanoscale, 2014, 6, 1763–1774.

55 H. Zeng, W. Cai, Y. Li, J. Hu and P. Liu, J. Phys. Chem. B, 2005, 109, 18260–18266.

56 L. Yang, P. W. May, L. Yin and T. B. Scott, Nanotechnology, 2007, 18, 215602.

57 H. Zeng, X. Ning and X. Li, Phys. Chem. Chem. Phys., 2015, 17, 19637.

58 K. A. Alim, V. A. Fonoberov, M. Shamsa and A. A. Balandin, J. Appl. Phys., 2005, 97, 124313.

59 R. H. Callender, S. S. Sussman, M. Selders and R. K. Chang, Phys. Rev. B: Solid State, 1973, 7, 3788.

60 Z. Q. Chen, A. Kawasuso, Y. Xu, H. Naramoto, X. L. Yuan, T. Sekiguchi, R. Suzuki and T. Ohdaira, J. Appl. Phys., 2005, 97, 013528.

61 J. N. Zeng, J. K. Low, Z. M. Ren, T. Liew and Y. F. Lu, Appl. Surf. Sci., 2007, 362, 197.

62 P. K. Giri, S. Bhattacharyya, D. K. Singh, R. Kesavamoorthy, B. K. Panigrahi and K. G. M. Nair, J. Appl. Phys., 2007, 102, 093515.

63 X. Li, J. Song, Y. Liu and H. Zeng, Curr. Appl. Phys., 2014, 14, 521–527.